Taylor & Francis
Taylor & Francis Group

Check for updates

Hydrodynamic optimality of balistiform and gymnotiform locomotion

Brennan Sprinkle[a] , Rahul Bale[b], Amneet Pal Singh Bhalla[b],
Malcolm A. MacIver[b,c,d] and Neelesh A. Patankar[a,b]

[a]Engineering Sciences and Applied Mathematics, Northwestern University, Evanston, IL, USA;
[b]Department of Mechanical Engineering, Northwestern University, Evanston, IL, USA; [c]Department of
Biomedical Engineering, Northwestern University, Evanston, IL, USA; [d]Department of Neurobiology,
Northwestern University, Evanston, IL, USA

ABSTRACT

Some groups of fish have evolved to generate propulsion using undulatory elongated fins while maintaining a relatively rigid body. The fins run along the body axis and can be dorsal, ventral, dorsoventral pairs or left-right pairs. These fish are termed as median/paired fin (MPF) swimmers. The movement of these groups of fish was studied in an influential series of papers by Lighthill and Blake. In this work, we revisit this problem by performing direct numerical simulations. We interrogate two issues. First, we investigate and explain a key morphological feature, which is the diagonal fin insertion found in many MPF swimmers such as the knifefish. Not only are these results of biological relevance, but these are also useful in engineering to design bioinspired highly maneuverable underwater vehicles. Second, we investigate whether there is a mechanical advantage in the form of reduced cost of transport (COT) (energy spent per unit distance traveled) for not undulating the entire body. We find that a rigid body attached to an undulating fin leads to a reduced COT.

1. Introduction

In this work, we examine the physics of swimmers who hold a part of their body rigid and use an affixed, undulatory fin for propulsion. Some examples of these types of swimmers include: knifefish, triggerfish, bowfin and oarfish (cf. Figure 1). Swimmers who fit this description may be classified as undulatory median/paired fin (MPF) swimmers. These are swimmers who propel themselves by undulating axial fins that are dorsal, ventral, dorsoventral pairs or left-right pairs. Among these swimmers are the gymnotiformes, who only undulate one elongated fin, and the balistiformes, who undulate a pair of anal and dorsal fins. In this work, we consider gymnotiform and balistiform swimmers.

CONTACT Neelesh A. Patankar ✉ n-patankar@northwestern.edu
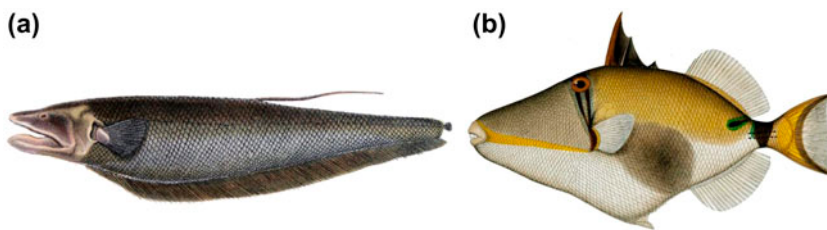
Figure 1. (a) *Apteronotus bonapartii*, a typical example of a gymnotiform swimmer. (b) *Rhinecanthus verrucosus*, a typical example of a balistiform swimmer.

Lighthill (1971) developed large-amplitude elongated-body theory which was later applied to gymnotiform (such as knifefish) and balistiform (such as triggerfish) swimmers in a series of four papers (Lighthill & Blake, 1990; Lighthill, 1990a, 1990b, 1990c). One of the questions they interrogated was whether there is any mechanical advantage when gymnotiform and balistiform swimmers hold their bodies nearly rigid while undulating their elongated fins. They developed a mathematical formulation for the thrust component of the axial (parallel to the base of the fin) force generated by elongated fins of gymnotiform and balistiform swimmers, pictured in Figure 1. Their Lighthill and Blake (1990) formulation uses a potential flow assumption and an approximate two-dimensional motion. They concluded that the thrust produced by elongated fins of balistiform or gymnotiform swimmers is increased due to the presence of a non-deforming (rigid–like) body attached to the fin. This, they hypothesised, would give the fish a mechanical advantage for holding their bodies rigid. In an earlier work (Bale et al., 2014), we studied this issue by performing numerical simulations and found no support for thrust enhancement for typical parameters of interest.

In this work, we perform numerical simulations of the model swimmers considered by Lighthill and Blake (1990) using the constraint–based immersed body (cIB) method by Bhalla, Bale, Griffith, and Patankar (2013) to the hydrodynamic forces and flow features produced by gymnotiform and balistiform swimmers. Specifically, we consider two issues. First, we investigate a key morphological feature, which is the diagonal fin insertion found in many MPF swimmers such as the knifefish (cf. Figure 1). Second, we investigate whether there is a mechanical advantage, in the form of reduced cost of transport (COT), (energy spent per unit distance travelled) in maintaining a rigid portion of the body.

In our investigation, we find that the resultant propulsive force generated by the elongated fin is at an angle to the fin axis. This is because the fin produces axial (parallel to the base of the fin) as well as heave (perpendicular to the base of the fin and in the plane of the body) force. The angle of the resultant force is found to be qualitatively consistent with the angle at which the fin is attached to the body (angle of insertion) of gymnotiform swimmers. The analysis by Lighthill and Blake (1990) did not account for the heave force. Hence, the issue of the angle of insertion of the fin could not be addressed by their analysis. We also perform

free swimming simulations to determine whether it is advantageous for MPF swimmers to hold their body rigid and undulate only their elongated fins. We conclude that there is a mechanical advantage to rigid–body swimming through a different metric than that proposed earlier (Lighthill & Blake, 1990).

2. Fin-plate fish model

Lighthill and Blake (1990) model balistiform swimmers with the body of the swimmer as a flat plate with undulatory fins attached at the top and bottom of the plate. They model the undulations of the fin by considering the motion of slices of the swimmer in a 2D plane intersecting the body at a right angle to the rostrocaudal axis. In one of these slices, the body is represented as a vertical line and two angled lines affixed to the top and bottom, representing the fins, which are oscillating at an angular frequency ω (a single fin version of this model can be seen in Figure 2(b)). A travelling wave progressing from front to back (single fin version seen in Figure 2) is then approximated by considering the motion of the fins in each slice to be slightly lagged from the slice in front of it. The model for a gymnotiform swimmer was the same except there was a fin only at the bottom end of the plate as shown in Figure 2(b).

In what follows, we only consider the full three-dimensional motion of a fin-plate model of a gymnotiform swimmer (Figure 2). The undulations of the fin will be modelled by a travelling sinusoidal wave. Like Lighthill and Blake (1990), we model the body of the swimmer as a flat plate while the displacement and the corresponding velocity of lateral undulation of the fin are given by

$$\theta = \theta_{\max} \sin\left[2\pi\left(\frac{x}{\lambda} + ft\right)\right], \tag{1}$$

$$V_w = 2\pi f \theta_{\max} r \cos\left[2\pi\left(\frac{x}{\lambda} + ft\right)\right], \tag{2}$$

respectively, where x is the axial-direction, θ is the angular excursion of the fin (Figure 2), $\theta_{\max}$ is the peak amplitude, λ is the wavelength, f is the frequency of undulation, V_w is the lateral speed at any location (x, r) on the fin, and r, which varies from 0 to h (the height of the fin), is the radial distance from the base of the fin at any x location. The speed with which the undulatory waves move along the fin, from head to tail (rostrocaudal direction, Figure 2), is the wave speed given by $U_w = f\lambda$. The coordinate axes are chosen such that the fin axis and the wave motion of the fin are along the x-axis, and the lateral direction is along the y-axis. Positive x is in the front-to-back direction, positive z is in the upward direction, and the positive y direction follows according to the right hand rule.

Refer to Figure 2 for the sign convention (demarcated by a '+' where appropriate). The forward swimming direction is taken to be caudorostral. Translational velocity U, of the swimming body or the fin, is positive if directed forward. The wave velocity U_w is positive in the rostrocaudal direction. According to the decoupled drag–thrust model, the axial force on an elongated fin is composed of
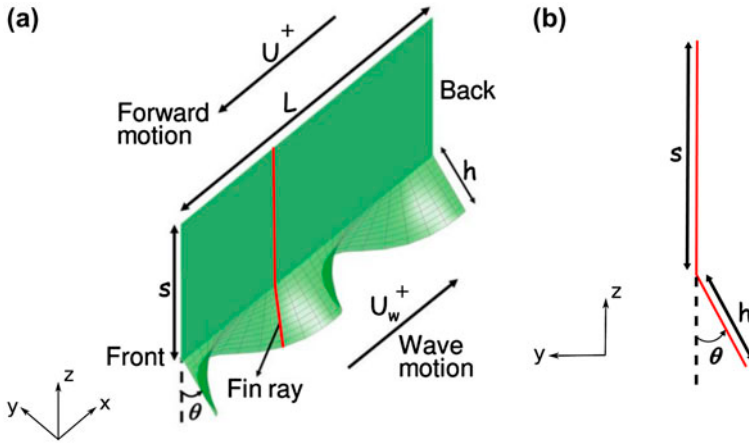
Figure 2. (a) 3D model of a gymnotiform swimmer considered in this work based on a prior study Lighthill and Blake (1990). *L* is the length of the body, *s* is the height of the plate, *h* is the height of the fin, U_w is the wave speed of the fin and *U* is the forward motion of swimmer. (b) cross-sectional slice of the 3D swimmer is shown in (a).

a thrust component and a drag component (Bale et al., 2014). The forward axial *thrust* force on the fin is positive (same sign as *U*) while the backward axial *drag* force on the fin is also positive (same sign as U_w). The resultant axial force *on the fin* (= thrust–drag) is positive toward the front. By action–reaction, the positive sense of forces *from the fin on the fluid* are reversed. In addition to the axial force, the elongated fin also generates a heave force due to its flapping motion. The heave force is positive when directed towards the base of the fin (positive *z* direction in Figure 2). Thus, the net propulsive force generated by an elongated fin is a resultant of the net axial force (= thrust–drag) and the heave force (a point which will be discussed in greater detail in Section 4).

3. Numerical problem formulation

The numerical simulations performed here are similar to those performed in our prior work (Bale et al., 2014). The swimmer is modelled as a thin membrane as described in Section 2 and the cIB method – see Bhalla et al. (2013) for details – is used to perform the simulations for given input data. Wall (zero velocity of all components) boundary conditions in all directions are used in the simulations performed in Sections 4 and 5, and wall boundary conditions in *y* and *z* directions with periodic conditions in *x* direction were used in the simulations for Section 6. The size of the computational domain, in all simulations performed in this work, was chosen through numerical trials to minimise the influence from the boundaries on the result. To this end, the exact choice of boundary conditions in each particular case did not significantly impact the results (less than $5 - 10\%$). In all simulations performed in this work, grid spacing at the finest level of the adaptive mesh in the Eulerian domain was chosen through numerical trials, so that the relative difference in

the force calculated by two successively refined simulations was lower than 5%. The spacing of the Lagrangian nodes representing the swimmer was chosen, so that the Eulerian cells which coincided with the swimmer contained, on average, one Lagrangian node. This follows the recommendation of Bhalla et al. (2013). Similarly, time steps were chosen for each simulation in such a way that the relative difference in the force calculated by two successively refined simulations wereas lower than 5%. In all simulations performed, the mean forces, steady swimming velocity and power of the fin were calculated as the time average over at least one period of oscillation, after a quasi-steady state is reached. The 'quasi-steady' regime is identified when the average over one or more periods of oscillation produces the same result to within 1%. Similar to our prior simulations Bale et al. (2014), two main types of simulation were performed in this work. For simulations performed in Section 4, computations were performed in the swimmer's reference frame, and hence, the swimmer was fixed in the computational domain and undulatory kinematics were prescribed, while for those of Section 5 and 6, only the deformation kinematics of the fin are prescribed, which results in a self-propelling fin-plate assembly. The density and viscosity of water were taken as $\rho = 1,000 \, \text{kg/m}^3$ and $\mu = 8.9 \times 10^{-4} \, \text{kg/m-s}$.

4. Relative importance of the components of propulsive force

We first examine different flow fields created by an undulatory fin. Specifically, we look for cross-sectional and axial flow fields. The flow field created by an undulating elongated fin that circulates in a plane perpendicular to the rostrocaudal axis of the swimmer (see Figure 3(c) for example) is termed as the cross-sectional flow field. Flow field in the axial direction is termed the axial flow field. In what follows, we will see that the axial force of a swimmer correlates to a circulating flow field along the length of the swimmer (Neveln et al., 2014; Shirgaonkar, Curet, Patankar, & MacIver, 2008) (see Figure 3(b) for example). We will also further investigate and quantify exactly when a cross-sectional flow field or an axial flow field represents the dominant pattern.

For the analysis in this section, we perform our simulations of the elongated fin only. For the computation of a fin's propulsive force, the physical parameters of interest are: L (length of the fin), h (height of the fin), θ_{max} (angular amplitude), λ (wavelength) and f (frequency). For our simulations, we fixed frequency $f = 1$ Hz, angular amplitude $\theta_{max} = 30°$. We chose these values as they have been shown Ruiz-Torres, Curet, Lauder, and MacIver (2012) to be typical, though at slightly reduced frequency than typically found for computational expedience. Further Bale, Bhalla, Neveln, MacIver, and Patankar (2015) and Shirgaonkar et al. (2008) show that any choice of f and any choice of $\theta_{max} > 20°$ should not affect trends in relative scaling of these forces with respect to other kinematic or morphological parameters. We introduce the following non-dimensional parameters: aspect ratio $AR = h/L$ and number of undulations $N = L/\lambda$. A
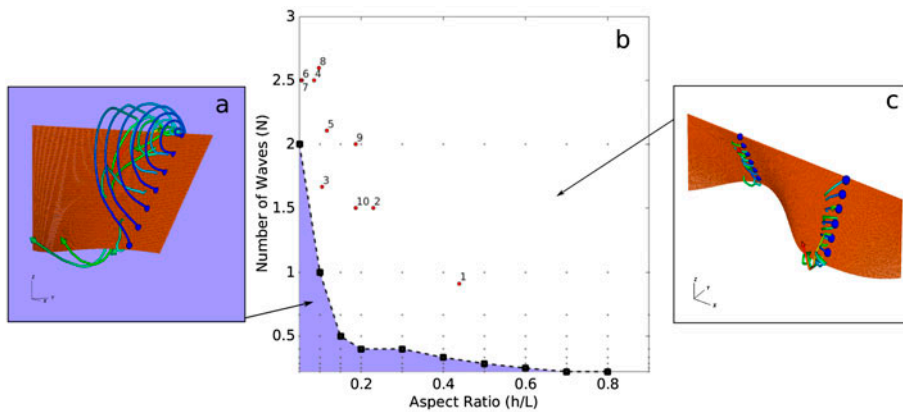
Figure 3. (b) The blue region represents the parameter regime in which the heave force is greater than that of the axial and in the white region, axial is greater than heave. The black squares and dashed line represent the computed boundary between these two regions. The error computed by increasing the resolution of the simulations for the data points nearest the boundary line (black squares) is within a 10% margin. The small grey dots indicate parameter values for which simulations were performed.

Notes: Finally, numbered points indicate the experimentally obtained parameter pairs corresponding to some select elongated fin species as follows: 1. *Rhinecanthus aculeatus*: Loofbourrow (2009) 2. *Sepia officinalis*: Bale et al. (2015) 3. *Xenomystus nigri*: Bale et al. (2015) 4. *Apteronotus leptorhynchus*: Bale et al. (2015) 5. *Amia calva*: Jagnandan and Sanford (2013) 6. *Gymnotus carapo*: Bale et al. (2015) 7. *Gymnorhamphichthys hypostomus*: Bale et al. (2015) 8. *Apteronotus albifrons*: Albert and Crampton (2005), Ruiz-Torres et al. (2012) 9. *Pseudobiceros bedfordi*: Bale et al. (2015) 10. *Pseudobiceros parladis*: Bale et al. (2015) We note that the kinematic parameters, such as f and θ_{max}, which were fixed in these simulations, vary for the different species shown. Thus, the animal data are shown for qualitative comparison only. (c) The flow field around a swimmer in the parameter regime where axial force dominates. Note the streamlines spiral along rays of the fin forming an axial flow field. (a) The flow field around a swimmer in the parameter regime where heave force dominates. Note the cross-sectional flow field.

physically realistic range for number of undulations is between $N = .2$ and 2 (Ruiz-Torres et al., 2012) and a physically realistic range for aspect ratios is those greater that $AR = .1$ (Albert & Crampton, 2005; Crampton & Albert, 2006). Further, we will use $AR = .9$ as an upper limit in our simulations as this seems to safely capture all fish morphologies we are interested in and reduces number of simulations needed to populate our study. Simulations of the elongated fin were carried out for these ranges of the AR and N. For each parameter pair considered, the axial and heave forces were computed.

The parameter space in which the axial force or the heave force is greater is shown in Figure 3(a). Further, within these regions, there is a correspondence with the dominant flow field being axial (in the cases where axial force is greater) or cross sectional (in the cases where heave force is greater). Thus, the heave force is more dependent on cross-sectional flow fields and the axial force is more dependent on axial flow fields. A point which is substantiated by Zhu, Wolfgang, Yue, and Triantafyllou (2002) for the axial force. Figure 3 shows that the axial force relative to the heave force is dominant at large AR. This is because taller fins at high AR are able to transport the fluid axially backwards more effectively giving rise to a more dominant axial flow field and axial force.

We see that there are physically realistic cases in which the cross-sectional flow field is the dominant flow feature. These cases represent a nearly 'flapping fin'
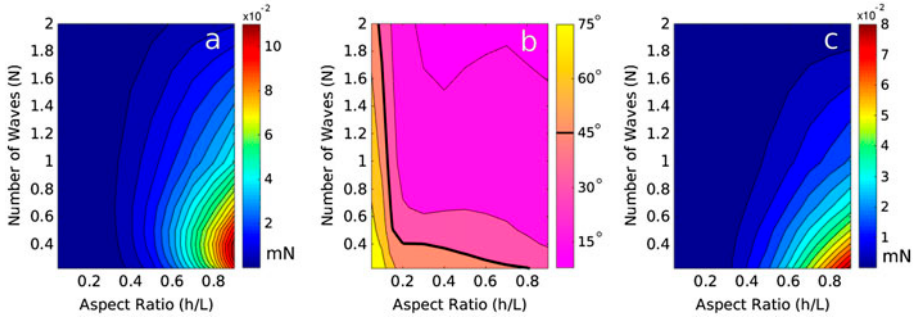
Figure 4. (a) Contour plot of simulated axial force (mN) data. (b) Angle ϕ (in degrees), of the resultant propulsive force generated by the fin with respect to the base of the fin. (c) Contour plot of simulated heave force (mN) data.

(similar to that of Figure 3(c)). This 'flapping fin' corresponds to the simplified model considered by Lighthill and Blake (1990). However, typical elongated fins have N and AR values that lie in the domain where axial forces and flows dominate as seen from data for elongated fin swimmers in Figure 3(a). This is consistent with experimental results (Neveln et al., 2014). Cases where the axial flow field and the axial force are dominant is the more physically prevalent scenario. The cross-sectional flow field assumed by Lighthill and Blake (1990), for axial thrust calculations, in fact corresponds to the, typically, sub-dominant heave force. Further, Lighthill and Blake (1990) did not consider heave force in their analysis. If a rigid body were attached to the fin, it is reasonable to expect that the axial flow caused by the fin would not be significantly altered compared to a case where there is no body attached to the fin. This is because the attached body would not disrupt the axial flow caused by the fin. Since our results show that the axial force correlates with the axial flow features, it may be deduced that the axial force too would not be significantly altered if a body were attached to the fin.

More than simply considering which flow field is dominant, we may also quantify their relative contribution to propulsive force. For this, we consider the net propulsive force on a swimmer as the vector sum of the axial and heave forces, which, in the cases considered above, will produce an angled propulsive force relative to the top edge of the elongated fin. This angle, ϕ, is computed as

$$\phi = \tan^{-1}\left(\frac{F_H}{F_A}\right),\qquad(3)$$

where F_A is the axial force and F_H is the heave force generated by the elongated fin. ϕ is a measure of the relative importance of axial and heave forces. That is, if heave is much greater than axial force, $\phi \approx 90°$; if the opposite is the case, then $\phi \approx 0°$; and if they are about the same, $\phi \approx 45°$. Figure 4 shows ϕ along with corresponding contours of axial and heave forces separately. The potential influence of this angle on fish morphology will be considered in the next section.
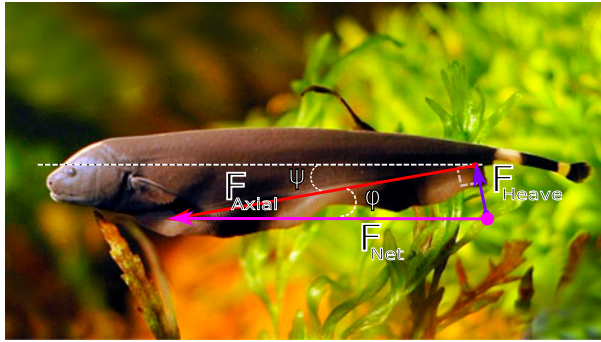
Figure 5. Angle ψ, called the angle of insertion of the fin, at which an elongated fin is attached to the body of a black ghost knifefish (photograph courtesy of Per Erik Sviland).

Notes: Also, shown is the angle ϕ of the resultant propulsive force generated by the fin with respect to the base of the fin. The fish will swim along an axis parallel to its rostrocaudal axis (e.g. the dashed grey line) if $\psi \approx \phi$. Forces shown are those acting from the fluid on the fin.

5. Angle of insertion of elongated fins

In the previous section, we focused our attention on which of these forces – axial or heave – is greater and how that corresponds to the dominant flow features. In general, both, cross-sectional and axial flow features are present, and hence, both axial and heave forces are produced. Although the axial force is typically dominant, in this section we demonstrate computationally that the heave force very likely influenced the morphology of MPF swimmers as discussed in the literature (Blake, 1983; Breder, 1926; MacIver, Fontaine, & Burdick, 2004; Sfakiotakis, Lane, & Davies, 1999). Since Lighthill and Blake (1990) did not model the heave force, the issue discussed here was not resolved in their work.

   All gymnotiform and balistiform swimmers have their undulatory fins attached to their rigidly held bodies at some angle, which we will call as the angle of insertion, ψ. Gymnotiform species, such as the black ghost knifefish, shown in Figure 5 have a non-zero angle of insertion. We hypothesise that, if a gymnotiform fish, which does not have paired fins, is to swim along an axis parallel to its backbone (straight forward swimming) without using other fins, then the angle ϕ (see Section 4) would be nearly equal to the angle of insertion ψ of the fin.

   Consider the black ghost knifefish, *Apteronotus albifrons*, (Figure 5), which has $N = 2.6$ and $AR = .1$ (Albert & Crampton, 2005; Ruiz-Torres et al., 2012). We measured the angle of the fin base with respect to the horizontal. This required determining the position of the horizontal axis through the body when the fish was swimming. We recorded video of the black ghost knifefish to determine the pitch of the body during straight forward swimming in flowing and still water. After orienting side view photographs to this pitch, we measured the angle of the fin base with respect to the horizontal. The black ghost knifefish data showed that the angle ψ for this fish is $9 \pm 2°$ (mean and std., sample size = 6) indicating that, in fact the axial force generated by the fin must be *dominant* for these

swimmers. However, the data shown in Figure 4 do not quantitatively show that $\psi \approx \phi$ for this swimmer. This is, in part, due to the different frequency of undulation between the simulations of Section 4 and the observed values for black ghost knifefish. In addition, the simulations in Figure 4 were for force generated by a fixed fin whereas in case of a swimming fish the elongated fin is translating at the speed of the fish. Hence, no matter the kinematic parameters, the agreement between ϕ and ψ can only be qualitative. From prior observations (Blake, 1983; Ruiz-Torres et al., 2012; Shirgaonkar et al., 2008), we may extract the broadest range of admissible swimming frequencies for the black ghost knifefish as $f = 3 - 15$ Hz, with normal cruising in the $f = 3 - 6$ Hz range. As evidence for the effect of frequency, we performed a simulation similar to those done for Figure 4 but used $f = 5$ Hz. This gives $\phi \approx 15.6°$ which is closer to 9° but still quantitatively off by roughly 70%. In order to resolve this further, we resort to more realistic, free swimming simulations.

To interrogate whether the observed angle of insertion of the fin ψ is consistent with the angle ϕ of the resultant propulsive force while swimming, we performed self-propulsion simulations of a black ghost knifefish using body geometry data that was experimentally extracted by Ruiz-Torres et al. (2012) and prescribed fin kinematics were taken as $f = 3$ Hz and $\theta_{\max} = 30°$. The exact value for frequency was chosen to be in the admissible frequency range for the black ghost knifefish and also to minimise computational expense. If our hypothesis that $\psi \approx \phi$, *while swimming*, is correct, then the computational fish will swim straight ahead when the fin is attached to the body at an angle of 9°. This is indeed observed in self-propulsion simulation results in Figure 6. All rotational degrees of freedom were locked in the self-propulsion simulation results of Figure 6 in order to prevent the fish from pitching or rolling. Pitching and rolling moments may be countered by real fish using pectoral fins. Based on the simulations while we cannot say that the body will not pitch, we can say that the absence of vertical displacement during forward swimming supports our claim that ψ is consistent with ϕ.

To further verify that this straight, forward motion is caused by a *balance* of axial and heave forces, we reverse the motion of the fin undulations midway through the simulation. If, the angle of the fin is balancing heave and axial forces, we should then see the swimmer reverse at an angle of roughly 2ψ relative to the swimmers midline (assuming force magnitudes are relatively same during backward motion). In Figure 6, we see that this is indeed the case and is also consistent with experimental observations (MacIver et al., 2004). This tells us that the angle which a gymnotiform swimmer's elongated fin makes to its midline can be used as a gauge for how much heave vs. axial force it is generating.

6. Is there a mechanical advantage due to a body held rigid?

We simulate a model problem by considering a rectangular sheet of height H and length L as the 'body.' Given this body, we consider different cases by varying
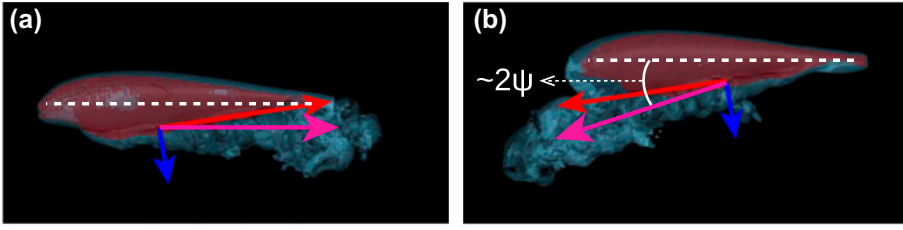
Figure 6. Snapshots of forward swimming (a) and backward swimming (b) simulated black ghost knifefish.
Notes: Shown in each panel, are iso-surfaces of the magnitude of vorticity for flow visualisation. Figures show that the wake structures shed from the fin line up with the net force vector. Specifically, for a backward swimming fish in (b) the wake structures shed from the fin line up with the net force vector at an angle of roughly 2ψ or 18° relative to the swimmers midline.

the fin height, h, (or equivalently plate height, s) but keeping a fixed total height $H = h + s$. In what follows, the fin is undulated at $f = 3$ Hz and with $\theta_{max} = 30°$. Further in an attempt to keep our results as general as possible when fixing a parameter, we chose to fix the specific wavelength

$$SW = \frac{\lambda}{\frac{h}{2}\sin(\theta_{max})}, \tag{4}$$

at $SW = 20$ as this was found to hold for elongated fin swimmers (Bale et al., 2015). Self-propulsion simulations were performed. The average power P_{avg} expended by the fin over one period of the swimming cycle and the average steady swimming speed U_s were calculated. A COT metric defined by

$$COT = \frac{P_{avg}}{U_s}, \tag{5}$$

was calculated. Then we investigated whether, for a given body (i.e. H and L specified), there is a fin height h that minimised COT. The goal was to find 'optimal' (defined as the one that minimises COT) swimmer dimensions as a function of the aspect ratio $A_r = H/L$. Note that this definition differs from the aspect ratio (AR) considered in Section 4 as A_r is the body aspect ratio, while AR is the *fin* aspect ratio.

To collect our desired data, we performed four sets of simulations. For a fixed total swimmer body height of $H = 1$ cm in all cases considered, we simulated four different fin lengths, $L = 10, 5, 2.5$ and 1.25 cm. These represent aspect ratios of $A_r = .1, .2, .4$ and $.8$, respectively. For each length value, we considered several fin height values in the range $h = .1$ to 1.0 cm. All data collected from these simulations have less than a 10% margin of error based on grid sensitivity.

In Figure 7, we have plotted the COT curves of different length swimmers as functions of fin heights. We see a clear separation of trends. In the two smallest aspect ratio cases ($A_r = .1, .2$), there is one pronounced minimum around $h = .2$ cm in both cases, and the COT increases monotonically for $h > .2$ cm. Further, we note that the COT data for these two lowest aspect ratio cases,
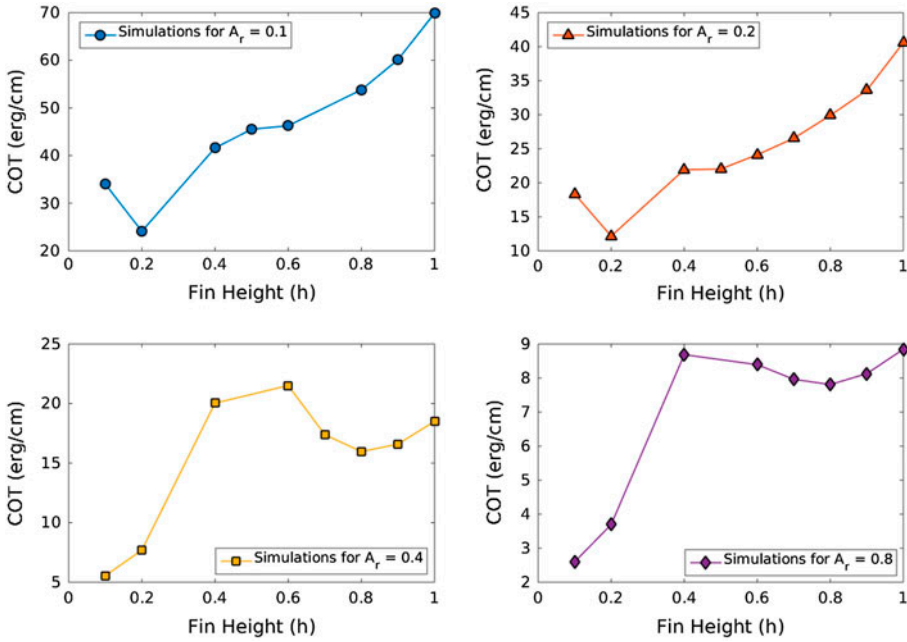
Figure 7. The results of our numerical simulations for different length swimmers are shown in the above 4 plots.

$A_r = .1, .2$, are in qualitative agreement with the COT data presented in Bale et al. (2014). By contrast, the two largest aspect ratio cases both have minima at the smallest h values we could simulate (there were numerical convergence problems for smaller values of h) and less pronounced local minima at higher values of h ($h = .8$ cm in both cases).

We deduce that no matter the exact morphology of the 'gymnotiform-like' swimmer considered, it is mechanically advantageous to have a rigid body constitute part of the swimmer. This conclusion seems to suggest that a rigidly held body is more than a vessel for organs, it may provide some mechanical advantage as far as the COT is concerned. The reason for this advantage is hypothesised to be different scalings of drag and thrust forces on a undulatory propulsor similar to those discussed by Bale et al. (2014). A detailed investigation of how body size affects these drag and thrust scalings, along with a physical explanation, should be a subject of future work.

7. Conclusions

In this work, we show that for an elongated fin attached to a plate, the dominant flow field is often not cross sectional but axial, which is consistent with prior simulations and experiments (Neveln et al., 2014; Ruiz-Torres et al., 2012; Shirgaonkar et al., 2008). In fact, we found that both the flow pattern and the larger component of the propulsive force may change depending on the physical parameters of a gymnotiform swimmer and that this may have influenced the morphology of

some swimmers, i.e. the angle at which the elongated fin is attached to the body of the fish. We also found that there is a mechanical advantage (by minimising COT) to holding part of the body rigid as is observed in gymnotiform and balistiform swimmers.

Disclosure statement

No potential conflict of interest was reported by the authors.

Funding

ORCID

Brennan Sprinkle http://orcid.org/0000-0001-6005-1668

References

Albert, J. S., & Crampton, W. G. R. (2005). Diversity and phylogeny of Neotropical electric fishes (Gymnotiformes), Chapter 13, In T. H. Bullock, C. D. Hopkins, A. N. Popper, & R. R. Fay, (Eds.), *Electroreception* (pp. 360–409). New York, NY: Springer Handbook of Auditory Research.

Bale, R., Bhalla, A. P. S., Neveln, I. D., MacIver, M. A., & Patankar, N. A. (2015). Convergent evolution of mechanically optimal locomotion in aquatic invertebrates and vertebrates. *PLOS Biology, 13*, e1002123.

Bale, R., Shirgaonkar, A. A., Neveln, I. D., Bhalla, A. P. S., MacIver, M. A., & Patankar, N. A. (2014). Separability of drag and thrust in undulatory animals and machines. *Scientific Reports, 4*, 7329.

Bhalla, A. P. S., Bale, R., Griffith, B. E., & Patankar, N. A. (2013, October). A unified mathematical framework and an adaptive numerical method for fluid-structure interaction with rigid, deforming, and elastic bodies. *Journal of Computational Physics, 250*, 446–476.

Blake, R. W. (1983). Swimming in the electric eels and knifefishes. *Canadian Journal of Zoology, 61*, 1432–1441.

Breder, C. M. (1926). The locomotion of fishes. *Zoologica (N. Y.), 4*, 159–297.

Crampton, W. G. R., & Albert, J. S. (2006). Evolution of electric signal diversity in gymnotiform fishes. *Communication in Fishes, 2*, 647–731.

Jagnandan, K., & Sanford, C. P. (2013). Kinematics of ribbon-fin locomotion in the bowfin, *Amia calva. Journal of Experimental Zoology Part A: Ecological Genetics and Physiology, 319*, 569–583.

Lighthill, J. (1971, November). Large-amplitude elongated-body theory of fish locomotion. *Proceedings of the Royal Society of London. Series B, Biological Sciences, 179*, 125–138.

Lighthill, J. (1990a). Biofluiddynamics of balistiform and gymnotiform locomotion. Part 2. The pressure distribution arising in two-dimensional irrotational flow from a general symmetrical. *Journal of Fluid Mechanics, 213*, 1–10.

Lighthill, J. (1990b). Biofluiddynamics of balistiform and gymnotiform locomotion. Part 3. Momentum enhancement in the presence of a body of elliptic cross-section. *Journal of Fluid Mechanics, 213*, 11–20.

Lighthill, J. (1990c). Biofluiddynamics of balistiform and gymnotiform locomotion. Part 4. Short-wavelength limitations on momentum enhancement. *Journal of Fluid Mechanics, 213*, 21–28.

Lighthill, J., & Blake, R. W. (1990). Biofluiddynamics of balistiform and gymnotiform locomotion. Part 1. Biological background, and analysis by elongated-body theory. *Journal of Fluid Mechanics, 212*, 183–207.

Loofbourrow, H. (2009). *Hydrodynamics of balistiform swimming in the picasso triggerfish, rhinecanthus aculeatus* (Master's thesis). Vancouver: University of British Columbia.

MacIver, M. A., Fontaine, E., & Burdick, J. W. (2004). Designing future underwater vehicles: Principles and mechanisms of the weakly electric fish. *IEEE Journal of Oceanic Engineering, 29*, 651–659.

Neveln, I. D., Bale, R., Bhalla, A. P., Curet, O. M., Patankar, N. A., & Maciver, M. A. (2014, January). Undulating fins produce off-axis thrust and flow structures. *The Journal of Experimental Biology, 217*, 201–213.

Ruiz-Torres, R., Curet, O. M., Lauder, G. V., & MacIver, M. A. (2012). Kinematics of the ribbon fin in hovering and swimming of the electric ghost knifefish. *The Journal of Experimental Biology, 216*, 823–834.

Sfakiotakis, M., Lane, D. M., & Davies, J. B. C. (1999). Review of fish swimming modes for aquatic locomotion. *The IEEE Journal of Oceanic Engineering, 24*, 237–252.

Shirgaonkar, A. A., Curet, O. M., Patankar, N. A., & MacIver, M. A. (2008). The hydrodynamics of ribbon-fin propulsion during impulsive motion. *The Journal of Experimental Biology, 211*, 3490–3503.

Zhu, Q., Wolfgang, M. J., Yue, D. K. P., & Triantafyllou, M. S. (2002). Three-dimensional flow structures and vorticity control in fish-like swimming. *Journal of Fluid Mechanics, 468*, 1–28.